Galactic Emission Mapping at 5GHz
A User's Guide to the GEM Project
Senior Honors Thesis

Kate Marvel

July 22, 2003

Abstract

I present the background material and motivation for a new experiment to map the intensity and polarization of the galactic synchrotron foreground. This measurement is both useful in its own right and critical for observational studies of the cosmic microwave background radiation. After discussing the theoretical basis of CMB physics, I then outline the brief history of foreground observations. Next, I will present a design for a receiver designed to create a sky map at 5 GHz, and discuss considerations in its construction. Finally, I present a brief overview of the GEM computing system.

1 Introduction

In the past few years, exciting new developments in instrumentation and observational techniques have made the growing field of cosmology even more relevant to every branch of physics. Most importantly, the discovery of the cosmic microwave background radiation, or CMB, provides researchers with invaluable information about the young Universe. This radiation, characterized until quite recently as an unimportant background buzz, can be studied in depth, and small anisotropies in this primordial picture have enormous implications for our present-day Universe. Additionally, it is predicted that the CMB will be partially polarized as a result of quadrupolar anisotropies in the field, a result dramatically confirmed by the recent DASI experiment (Kovac et al., [8]). A picture of the polarized CMB, specifically the I, Q, and U Stokes parameters, will provide a snapshot of the exact conditions at the time of last scattering, when photons first decoupled from matter.

Because this radiation provides us with such a faint signal relative to other sources of emission, it is important to obtain an accurate picture of foreground sources. One of the most poorly understood components of this foreground emission is synchrotron radiation, or the acceleration of relativistic electrons in interstellar magnetic fields. While the mechanism of this acceleration is well known, estimates of the intensity and polarization of this radiation across the galactic plane suffer from uncertainties that limit the accuracy of current CMB maps. It is therefore necessary to obtain maps of galactic radiation at radio frequencies, where synchrotron radiation is dominant. GEM, the Galactic Emission Mapping project, seeks to generate these high-quality sky maps at a variety of radio frequencies. These maps provide useful information about the galaxy's emission at these wavelengths and serve as a valuable resource in studies of the cosmic microwave background radiation. By mapping the signals in the galactic region to a greater degree of accuracy than ever before, GEM provides a template that may be subtracted from CMB maps to obtain a better overall picture of the young Universe.

1.1 The Cosmic Microwave Background Radiation

To understand modern cosmology, it is important to know the implications of the Cosmic Microwave Background, alternately called the CMB or CBR. The CMB, one of the central predictions of standard Big Bang theory, is the result of matter decoupling from radiation in the early history of the Universe. In order for primordial nucleosynthesis to have happened on the expected timescale, theories locate this "last scattering surface" at redshift $z \approx 1100$, when $kT_{universe} \approx 1$ MeV (Smoot, [16]). The present CMB can be well-characterized as a thermal blackbody with peak $T = 2.73 \pm .001$ K ([16]).

1.2 Temperature Anisotropies

The measurement of deviations from isotropy in the CMB is well-studied, and there exists an enormous body of literature on the subject. The following will be a brief overview of the basic formalism for understanding the fluctuations in CMB radiation temperature and relating them to density perturbations in the early Universe.

The study of these density fluctuations is important for three main reasons (Smoot, [16]). First, deviation from isotropy in the temperature background is required in all theories of structure formation. By identifying the blotches in the sky where the temperature deviates a uniform value, we are in effect identifying the "seeds" of structure formation. Second, an accurate picture of the CMB is needed for confirmation of any theory dealing with early-Universe physics. All potential inflationary theories must agree with these observations, as must any workable quantum gravity theory. Finally, examining these imprints in the background gives us some insight into the large-scale topology and geometry of the Universe. The study of the anisotropies in the CMB was pioneered by NASA's COBE mission (Smoot et al., [17]), which detected anisotropies on the order of one part in 10^5.

At large angles, we can expand the relative variation in sky temperature in terms of the spherical harmonics $Y_{lm}(\theta, \phi)$:

$$\left(\frac{\delta T}{T}\right) = S(\theta, \phi) = \Sigma_l a_{lm} Y_{lm}(\theta, \phi). \quad (1)$$

Since this anisotropy is generated by random variations in an isotropic Universe, we can regard both S and a_{lm} as Gaussian random variables. Therefore, all information about the variation in the field can be obtained from the correlation function

$$C(\alpha) =< S(\mathbf{n})S(\mathbf{m}) >= \frac{1}{4\pi}\Sigma_l(2l+1)C_l P_l(\cos\alpha). \tag{2}$$

A dipole anisotropy ($l = 1$) has been observed; this is most likely completely due to the relative velocity of the observer. More important are observations at higher l. The power spectrum in l is fundamental to modern cosmology; it aids in breaking the degeneracies in various cosmological models.

1.3 Polarization

The gravitational instabilities that lead to temperature anisotropies in the CMB are also expected to lead to polarization of the radiation on the order of one part in 10^6. This CMB polarization is useful for several reasons (Kamionkowski, [6]). First, the presence of polarization is an important check of the basic assumptions of Big Bang cosmology. If the temperature anisotropies we observe are indeed imprinted on the surface of last scattering, we would expect these fluctuations to create an observable polarization pattern. Second, temperature anisotropies are subject to redshift caused by the expanding Universe, and so will be expected to evolve somewhat between last scattering and current observation. The polarization pattern, by contrast, is not expected to change significantly with time, and will therefore provide a more direct probe of last scattering. Finally, a polarization map can be decomposed into contributions from density fluctuations (scalar perturbations), vorticity or "eddies" at last scattering (vector perturbations) and contributions from gravitational waves (tensor perturbations) (Hu and White, [27]).

CMB polarization arises from quadrupole anisotropies at last scattering. In Thompson scattering, the electron oscillates in the direction of the incident light's electric field vector. This results in a scattering cross section that is dependent on polarization:

$$\frac{d\sigma_T}{d\Omega}\alpha|\hat{\epsilon}\cdot\hat{\epsilon'}|^2. \tag{3}$$

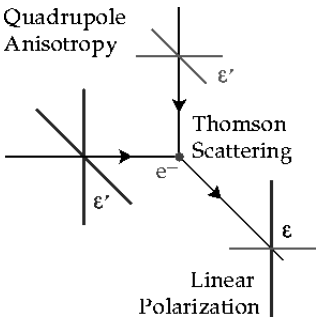

Figure 1: Thompson scattering by a quadrupolar temperature variation to create linear polarization. From Hu and White, http://background.uchicago.edu/ whu/polar/webversion/polar.html.

If the incoming radiation field were isotropic, peaks separated by 90° would cancel each other such that the outgoing radiation would remain unpolarized. However, if there exists a quadrupolar anisotropy in the temperature field such that there are intensity peaks separated by 90°, the outgoing radiation will be linearly polarized, as illustrated in Figure 1.

Signal polarization is generally discussed using the Stokes parameters I, Q, U, and V. The electric field components for a monochromatic plane wave propagating in the $\hat{z}$ direction are

$$E_x = a_x(t)cos[\omega t - \theta_x(t)] \quad E_y = a_y(t)cos[\omega t - \theta_y(t)]. \tag{4}$$

The sense of the polarization is determined by the phase differences θ. For complete linear polarization, the electric field points completely along the $\hat{x}$ or $\hat{y}$ direction. If, however, the waves are out of phase by 90°, we expect elliptical polarization. In the special case where $a_x = a_y$, we have circular polarization.

The Stokes parameters are defined as follows (Rybicki and Lightman [14]):

$$I =< a_x^2 > + < a_y^2 > \tag{5}$$

$$Q =< a_x^2 > - < a_y^2 > \tag{6}$$

$$U =< 2axa_y \cos(\theta_x - \theta_y) > \tag{7}$$

$$V =< 2a_x a_y \sin(\theta_x - \theta_y) > \tag{8}$$

It is not difficult to see that I is proportional to the total intensity of the wave. The V parameter is a measure of the "circularity" of the polarization. It is maximized for a phase difference of 90°. Thus, it is zero for a completely linearly polarized wave. Q and U measure the linear polarization of the wave (Rybicki and Lightman [14]). It can be shown that they transform under a rotation about the angle ϕ as

$$Q' = Q\cos(2\phi) + U\sin(2\phi) \quad U' = -Q\sin(2\phi) + U\cos(2\phi). \tag{9}$$

For the CMB, the polarization is generally regarded as a symmetric second-rank tensor on the sphere:

$$P_{ab} = \frac{1}{2}\begin{pmatrix} Q & -U\sin\theta \\ -U\sin\theta & -Q\sin\theta \end{pmatrix} \tag{10}$$

The invariant quantities are I, $Q + \imath U$, and $Q - \imath U$ (Sazhin[15]). These correspond to the total radiative intensity, and what we define as the E and B modes of polarization. Because polarization is a tensor, we cannot expand it as in Equation 1; however, we can use a set of *tensor* spherical harmonics:

$$P_{ab} = \sum_{l=2}\infty \sum_{m=-l} +l[a^E_{lm}Y^E_{(lm)ab} + a^B_{lm}Y^B_{(lm)ab}] \tag{11}$$

in the E and B modes (Balbi [1]). The dominant source of polarization is density perturbations; we expect this to contribute solely in the E mode (White [26]). The E mode is therefore coupled to the temperature field, while the B mode is independent. Smaller effects from vector and tensor perturbations will be expected to create a B-mode pattern.

1.4 Foregrounds

Studies of the CMB suffer from foreground contamination. Foreground emission is generally defined as any signal "whose dependence on cosmological parameters we cannot compute accurately from first principles at the present time" (Tegmark, [20]). While foregrounds can originate both in the Milky Way itself and from extragalactic sources, we will deal here with only the signals of galactic origin.

1.5 Galactic Emission

The dominant emission mechanisms in the Milky Way are dust, free-free emission, and synchrotron radiation. Interstellar dust contributes about 10-30% of the total

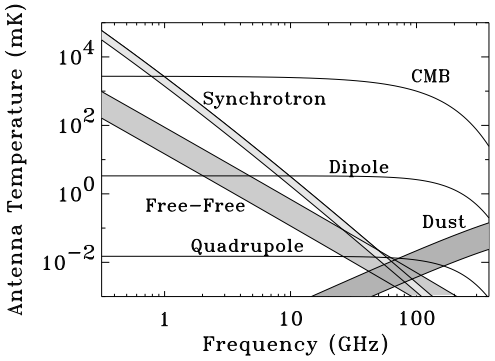

Figure 2: Frequency dependence of various galactic emission processes. Picture from [2].

emission from the galaxy (Banday, [2]), and is dominant in the infrared region of the spectrum. Dust emits as a blackbody modified by an emissivity that depends on frequency, Q_ν. The exact form of Q_ν is not precisely known; in general it depends on the atomic structure and composition of the dust grain itself. The temperature of the cosmic dust is generally on the order of 20K (Longair,[10]).

Free-free, or bremsstrahlung, emission from ionized hydrogen is dominant at frequencies between 20 and 60 GHz (Torres et al. [22]). It is thought that a full sky map in Hα will be beneficial to understanding the spatial dependence and absolute level of free-free emission; however, no such map presently exists (De Zotti et al., [3]).

Synchrotron radiation is the dominant component of galactic emission at radio frequencies. It arises from the spiraling of relativistic electrons about interstellar magnetic fields. In general, the intensity scales as a power law with the frequency. If the magnetic field strength is B, and the density of electrons is $N(E)dE$, then the intensity is given by

$$J_\nu \alpha N_o B^{(p+1)/2} \nu^{-\beta} \tag{12}$$

where $\beta = (p-1)/2$ is defined as the spectral index. Uncertainty in the frequency vari-

ation of the spectral index, as well as the location and strength of galactic magnetic fields, make an accurate map necessary for a complete understanding of synchrotron radiation.

For synchrotron radiation-dominated signals, we expect a high degree of polarization. Qualitatively, we expect the radiation from a single relativistic charge to be elliptically polarized. However, given a large, approximately isotropic distribution of charged particles, we would expect the elliptical component to cancel, yielding a linearly polarized signal. Following an argument in Rybicki and Lightman, the total polarization per unit frequency $\Pi(\omega)$ can be written in terms of the powers per unit frequency in directions parallel to and perpendicular to the projection of the magnetic field on the sky:

$$\Pi(\omega) = \frac{P_{\perp}(\omega) - P_{\parallel}(\omega)}{P_{\perp}(\omega) + P_{\parallel}(\omega)}. \tag{13}$$

Integrating over all frequencies yields an expected polarization of $\approx 75\%$. For particles with a power law distribution of energies, the degree of polarization can be expressed as

$$\Pi = \frac{p+1}{p+\frac{7}{3}}. \tag{14}$$

This means we can expect synchrotron radiation with a spectral index 3 to be about 75% polarized. However, there exist mechanisms in the Galaxy to unpolarize this radiation such that we expect only about a 30% polarized component.

2 Experimental Goals

The goal of the GEM Project is to produce a set of high-quality sky maps at various frequencies.

2.1 Intensity

It has been shown that the synchrotron spectral index varies with galactic latitude, highlighting the need for well-calibrated multifrequency maps at several frequencies (Torres et al., [23]). Except for the 408 MHz Haslam map (1982), there currently

exist only partial sky maps of the synchrotron background (Torres, [23]). Existing surveys suffer from uncertainty in gain calibration and an unknown absolute level of intensity. The Haslam map itself is patched together from several data sets and displays residual striping effects; this seriously limits the quality of the existing maps. GEM seeks to determine the following parameters to a high degree of accuracy:

- The spectral index of synchrotron radiation at 5 GHz.
- The location and strength of galactic magnetic fields. Because the synchrotron power emitted depends on the local magnetic field strength, a high-quality map will provide for more accurate studies of these field lines.
- The electron density variations across the galaxy.

Possible other uses for this data include galactic studies and tests of cosmic ray acceleration models ([23]).

2.2 Polarization

The polarization content of foregrounds is thus far relatively unknown, and presents a serious problem for the measurement of CMB polarization. Previous models have relied on low-frequency observations and on simulations; these are especially complicated by Faraday depolarization, which is dominant at lower frequencies ([20]). Measurements of the CMB polarization power spectrum suffer at low l; this complicates measurement of the expected "reionization bump" and the tensor B-modes, thought to peak at low$l$ ([20]). An accurate determination of synchrotron foreground is therefore very important for CMB polarization measurements. GEM aims to provide an accurate picture of the I, Q, and U Stokes parameters at 5 GHz.

3 Simulations

In order to determine the sensitivity needed to detect the polarization of the galaxy at 5GHz, we used simulations written by Domingos Barbosa, a former postdoctoral

researcher at LBL. His maps are made using templates produced by Giardino et al. using the Haslam 408 MHz and the Rhodes 2.326 GHz sky maps. To produce simulations for our purposes, Barbosa scaled down the maps to 5GHz from 30 GHz, degraded the pixel resolution to account for the GEM beam size, and took into account the GEM pointing. These results can be found on the GEM website at http://kepler.lbl.gov.

3.1 Simulation Results and Predictions

Our further work with the simulations involved using them to determine our needed sensitivity. First, we combined the maps and scaled them down as a check to Barbosa's assumptions. we then constructed a map to yield the total polarization expected. Binning the total polarization $\sqrt{Q^2+U^2}$ by half-degrees Kelvin yields the histogram in Fig. 3. Here, slightly less than 95% of the signal is above 1mK. This

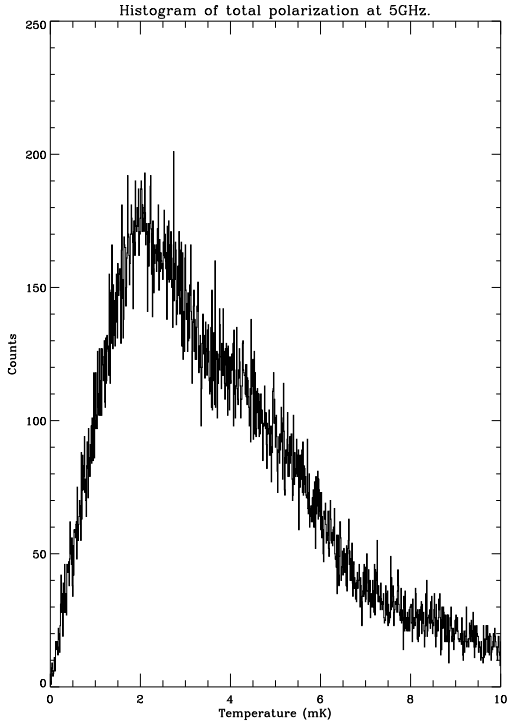

Figure 3: Total polarization temperature histogram.

indicates that our experimental goal will be designing a receiver sensitive to this

antenna temperature.

4 Receiver Design

To achieve these goals, the GEM project is currently designing a new receiver at 5 GHz to be placed in the GEM dish in Cachoeira Paulista, Brazil. The rotating dish scans the sky in 60° wide circles at 1 rpm, providing complete coverage of a 60° declination band (Tello et. al, [21]). The telescope is portable, allowing for coverage at several latitudes to map the entire sky.

4.1 Radio Astronomy Fundamentals

In astronomy, we are mostly concerned with the incident radiation power from some astrophysical source. For a radio telescope, this is generally measured by the temperature of the antenna, T_A. If the brightness temperature of a blackbody source is T_B and it subtends a solid angle of Ω_s, then

$$T_A \approx T_B \frac{\Omega_s}{\Omega_b + \Omega_s} \tag{15}$$

where Ω_b is the solid angle of the antenna beam. Thus, a small pointlike source will have a smaller effect on the antenna temperature then, for example, a nearby radiating body like the Sun (Heiles, [5]).

The antenna temperature is often tiny compared to the receiver's *system* temperature, $T_{sys} = T_A + T_R$. The receiver temperature, T_R is determined from the components of the signal chain, which all have an associated noise temperature. This is not necessarily the component's physical temperature. Most prepackaged components come with a quoted noise figure F, which is measured by connecting the device to a signal generator with known source impedance. If the output noise power due to the generator noise is W_{GN} and the noise power due to the component is W_N, then

$$F = \frac{W_{GN} + W_N}{W_{GN}}. \tag{16}$$

The noise temperature T of the component is defined as

$$T = \frac{W_N}{Gk\delta\nu} \tag{17}$$

where G is the gain of the component, k is Boltzmann's constant, and $\delta\nu$ is the bandwidth. Thus, we can get T from the noise figure F by writing

$$T = (F-1)T_0 \tag{18}$$

where T_0 is the ambient temperature. The noise temperature of the receiver is determined by cascading the noise temperatures of the individual components, most of which can be treated as linear two-ports (Kraus, [7]).

4.2 Expected Design

Our expected signal chain is shown in Figure 4. This design consists of two separate amplification chains for each circular polarization state. Because the signals in both chains are combined in the hybrid, the sensitivity improves by a factor of $\sqrt{2}$ [7]. Additionally, uncorrelated noise (i.e. random gain fluctuations) will disappear in the mixing process, decreasing the weight of the $\frac{\Delta G}{G}$ term in the sensitivity equation

$$\Delta T_{rms} = T_{sys}\sqrt{\frac{1}{\Delta\nu\tau} + (\frac{\Delta G}{G})^2}. \tag{19}$$

Depending on the relative phase differences, the outputs at the detector diodes are given by

$$\frac{G_1^2 + G_2^2}{2}\mathbf{I} + \frac{G_1^2 - G_2^2}{2}\mathbf{Q} \pm G_1G_2[\mathbf{U}\cos\Delta\phi - \mathbf{V}\sin\Delta\phi]; \tag{20}$$

assuming the gains of both chains are equal and the phases are chopped between 0 and 180 degrees, we can detect just I and U. We may rotate the entire setup 45 degrees to obtain Q instead. Digitally adding the outputs of both lock-ins gives $(G_1^2 + G_2^2)\mathbf{I}$; subtracting gives $2G_1G_2\mathbf{U}\cos\Delta\phi$.

4.3 Formalism

For an in-depth analysis of the signal chain, we turn to a polarimeter formalism developed in O'Dell ([11]).. In this system, the actions of radiometric components

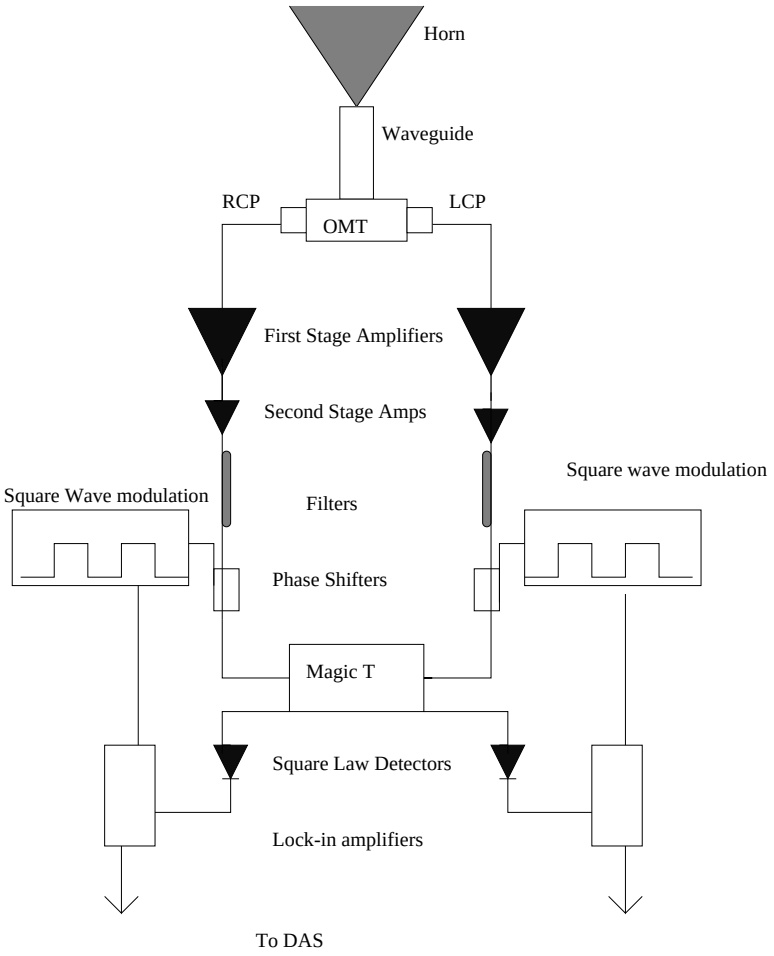

Figure 4: Expected receiver design.

are represented by matrix operators in the basis defined by the two orthogonal linear polarization states. The incoming signal is expressed in terms of these two states or as a real Stokes vector:

$$|E\rangle = e^{i(kz-\omega t)} \begin{bmatrix} E_{x_0} e^{i\phi_x} \\ E_{y_0} e^{i\phi_y} \end{bmatrix} = \begin{bmatrix} I \\ Q \\ U \\ V \end{bmatrix}. \tag{21}$$

The Stokes parameters $\mathbf{I}, \mathbf{Q}, \mathbf{U}, \mathbf{V}$ in this representation are given by

$$I = \begin{bmatrix} 1 & 0 \\ 0 & 1 \end{bmatrix} \quad Q = \begin{bmatrix} 1 & 0 \\ 0 & -1 \end{bmatrix}$$

$$U = \begin{bmatrix} 0 & 1 \\ 1 & 0 \end{bmatrix} \quad V = \begin{bmatrix} 0 & -i \\ i & 0 \end{bmatrix} \tag{22}$$

Each component acts upon the initial state, creating a new state $|E_{new}\rangle = \mathbf{M}\,|E_{initial}\rangle$.

In our proposed chain, the OMT separates two polarizations and sends them down two coaxial cables. These two polarizations, however, can be considered part of the same state, so we represent the action of the OMT by the identity matrix multiplied by a small gain term. The same goes for the filters, which should not affect the signal's representation in the polarization basis. The amplifiers do not mix the states, but they introduce a large gain term into the system. Likewise, the action of the phase shifters is represented by a matrix containing complex phase terms on the diagonal. The states are combined in the "magic T" and split again; one half is passed through unchanged, while the other is phase-shifted 180°. A summary of all components and their associated operators is shown in Table 1.

Unlike the other components, which create a new state vector, the output of the detector diodes is a scalar voltage. The formalism here is

$$\langle E_{in}|\,\mathbf{D}\,|E_{in}\rangle \tag{23}$$

where $|E_{in}\rangle$ represents the input state vector and $\mathbf{D}$ is the operator representing the action of the detector diode. Because we have one detector per receiver arm, these operators are

$$\mathbf{D} = \begin{bmatrix} 1 & 0 \\ 0 & 0 \end{bmatrix} \quad \text{and} \quad \mathbf{D} = \begin{bmatrix} 0 & 0 \\ 0 & 1 \end{bmatrix}$$

for the left and right hand sides of the diagram, respectively. Before the signal enters the detector diodes, its state vector is given by

$$|E_{in}\rangle = \mathbf{M_1 M_2} \ldots \mathbf{M_n}\,|E_{initial}\rangle \tag{24}$$

where $\mathbf{M_i}$ are the operators in Table 1. Acting on the new $|E_{in}\rangle$ with the diodes using Eqn. 23 yields the previously mentioned result in Eqn. 20.

Component Name	Operator Equivalent
Orthomode Transducer	$\begin{bmatrix} G_{OMT} & 0 \\ 0 & G_{OMT} \end{bmatrix}$
First Stage Amplifiers	$\begin{bmatrix} G_{amp1} & 0 \\ 0 & G_{amp1} \end{bmatrix}$
Second Stage Amplifiers	$\begin{bmatrix} G_{amp2} & 0 \\ 0 & G_{amp2} \end{bmatrix}$
Phase Shifters	$\begin{bmatrix} 1 & 0 \\ 0 & e^{i\Delta\phi} \end{bmatrix}$
Filters	$\begin{bmatrix} G_{filt} & 0 \\ 0 & G_{filt} \end{bmatrix}$
Magic T	$\frac{1}{\sqrt{2}} \begin{bmatrix} 1 & 1 \\ 1 & -1 \end{bmatrix}$

Table 1: Components and formalism. Table adapted from [11].

5 Components

5.1 Orthomode Transducer

An orthomode transducer is a device that splits an incoming signal into its right circularly polarized and left circularly polarized components. Understanding how it works requires a knowledge of waveguide and transmission line theory and basic electromagnetism. Heuristically, a waveguide's conducting sides impose boundary

conditions on the EM fields inside; by solving Maxwell's equations subject to these constraints we obtain the transmission behavior of the waveguide.

Inside a waveguide, the propagating waves may take one of two forms. If the electric field vector is transverse to the direction of motion, the wave is referred to as a TE (transverse-electric) mode; for a transverse magnetic field vector we have TM modes. Generally, these modes are written with subscripts as TE_{mn} and TM_{mn}; for circular waveguide the m denotes the number of full-wave variations of the radial component around the circumference of the guide. The subscript n indicates the number of half-wave variations across a diameter (Lance, [9]). The dominant mode in circular waveguide is the TE_{11} mode, but higher-order TE_{01} and TM_{01} modes are often present as well.

For a more complete treatment of the field inside a circular waveguide, I use the reasoning in Whinnery *et al.* (Whinnery,citewhin). Using the Helmholtz equations in cylindrical coordinates

$$\nabla_t E_z = \frac{1}{r}\frac{\partial}{\partial r}\left(r\frac{\partial E_z}{\partial r}\right) + \frac{1}{r^2}\frac{\partial^2 E_z}{\partial \phi^2} = -k_c^2 E_z, \tag{25}$$

the z-component of the electric field for TM waves is

$$E_z(r,\phi) = AJ_n(k_c r)\cos n\phi. \tag{26}$$

Using Maxell's equations, we can obtain the other field components from this result. Likewise, for TE waves imposing $E_z = 0$ yields

$$H_z(r,\phi) = BJ_n(k_c r)\cos n\phi. \tag{27}$$

The cutoff frequency f_c is the frequency below which the waveguide will act as an attenuator. For circular waveguide, the electromagnetic equations appear as Bessel functions, as shown above. The cutoff wavelength λ_c and the radius of the waveguide a are related by

$$\frac{2\pi a}{\lambda_c} = p_{mn} \tag{28}$$

where p_{mn} is the n^{th} root of the Bessel function $J_m(n) = 0$. This equation follows naturally from the condition that the electric field be zero at the conducting boundary.

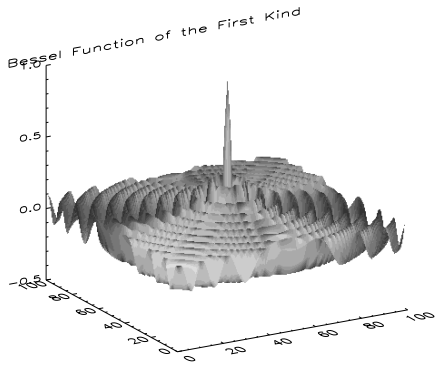

Figure 5: Bessel functions.

For the TE11 mode, we have

$$\frac{2\pi a}{\lambda_c} = 1.84. \tag{29}$$

The orthomode transducer consists of a circular section of waveguide short-circuited at one end by a reflective plate. This is depicted schematically in the CAD shown on the GEM website at *http://kepler.lbl.gov*. The plate is placed a half-wavelength from a junction where two small sections of rectangular waveguide are flanged to the body of the transducer in an orthogonal configuration. There is a quarter-wave plate inserted at a 45° angle to the axis defined by these waveguide branches.

To choose the dimensions for the waveguide itself, we want to adhere to industry-standard guidelines as much as possible. This will enable us to purchase waveguide components that we know will flange easily to SMA cable. For a 5 GHz center frequency, the standard rectangular waveguide is WR-187, which is 1' by 2", or 2.54 by 5.08 cm. We chose a circular waveguide diameter of one wavelength- 6 cm- so as not to attenuate any frequency within our bandwidth of 200 MHz. This means that the two rectangular waveguides must be placed 9.42 cm apart to receive orthogonal modes. The reflective plate is made of aluminum, silver, or some other highly reflective material, and placed $\frac{\lambda}{2} = 3$ cm from the axis defined by the orthogonal rectangular waveguides. This is connected to a "plunger" and can be adjusted for maximum power output. There is a quarter wave trap machined into the plunger to reduce

effects from stray waves that somehow leak out of the transducer.

The quarter-wave plate is a slab of Teflon. Because both right- and left- circularly polarized modes can be regarded as linear combinations of the two orthogonal linear polarization states, we know that at any fixed point in time both linear modes will be orthogonal to each other. Thus, if the plate is placed 45° from the axis defined by these modes, we can see that one mode will be normal to the plate, while the other will pass through. Teflon's dielectric constant is 2.1, which means that one mode will travel more slowly through than the other. If the length is chosen properly, the two waves will emerge in phase and hence linearly polarized. To choose this length, we use the relation

$$\delta\phi = l(k_1 - k_2) \tag{30}$$

where $k_1 and k_2$ are the constants of propagation for the two modes (Uher,[24]). The propagation constant for a mode in a waveguide with a dielectric slab is

$$k_{mode} = \frac{2\pi}{\lambda_0}\sqrt{1 - \left(\frac{\lambda_0}{\lambda_{cmode}}\right)^2}\left(1 - \frac{\nu_{mode}}{1 - \left(\frac{\lambda_0}{\lambda_{cmode}}\right)^2}\right) \tag{31}$$

where ν_{mode} is the shift in resonance frequency for the mode ([24]). For left- and right-circularly polarized modes, these are

$$\nu_{TE11\bigcirc} = 0.513(\epsilon - 1)\frac{t}{a} \tag{32}$$

and

$$\nu_{TE11\bullet} = 0.331\frac{(\epsilon - 1)}{2\epsilon}\frac{t}{a} \tag{33}$$

where t and a denote the dielectric slab thickness and the diameter of the waveguide, respectively. Choosing $t = .3$ cm and $a = 6$ cm, we get a required length of 5.50 cm. This wave plate is diagrammed on the GEM website. The tapered edges are meant to reduce residual leakage effects.

5.2 Amplifier Chains

Our first-stage amplifiers will be cryogenic GaAs FET models from Miteq, inc. Briefly, these use transistors in feedback loops to ensure the impedance is matched to 50Ω.

Their quoted gain is 33 dB, and they are designed to operate at a temperature of 77K. To achieve this environment, they will be immersed in a liquid nitrogen dewar and shielded from external vibrations.

No component is perfect, and we expect every part of our signal chain to contribute somewhat to the system temperature T_{sys}. Because the amplifiers are immersed in liquid nitrogen, their ambient temperature T_0 is less than the standard 290 K. Using Equation 18 with the quoted noise figure of 0.2 dB, we estimate a noise temperature of 14.9 K.

Upon tests of the first stage amplifiers, we obtain the following parameters. Assuming a 1dB error due to instrument age, these values fall perfectly withing

Amplifier	Gain	Insertion Loss	Noise Temperature (77K)
1	34.3	.81	15.8
2	34.5	.80	14.9

acceptable limits.

The second-stage amplifiers will be purchased from Quinstar, Inc. Assuming maximum loss, we calculate a noise temperature of 169 K at 290 K ambient temperature.

5.3 Filters

The filter defines our bandwidth at 200 MHz. The filter we are purchasing has insertion loss $\leq$1.5dB at the 5 GHz center frequency. The manufacturer is Trilithic; price is \$895 each. Assuming maximum loss gives a noise temperature of $\approx$120K. The filter will be placed before the second stage amp to avoid amplifying too large a bandwidth. All second-stage components will be placed in an RF-tight box on the side of the dewar.

5.4 Phase Shifters

We are planning to purchase phase shifters from Miteq.,Inc. Ideally, we want rapid phase chops between 0° and 180° at about 100 Hz (i.e. much faster than the sky scan rate). This would mean we have to be sure to isolate these from other components to avoid introducing vibrational noise into the system. This chopping will serve to modulate the signal; it will be demodulated in the lock-in amplifiers following the detector diodes. Lock-in amplifiers have the capability of improving signal-to-noise ratio up to 60dB or more; we will have to investigate this property more thoroughly. Phase shifters seem to vary wildly in loss and VSWR; the best we've seen is the bi-phase modulator from KDI. This one uses TTL logic to switch phases between 0° and 180° at 100 Hz. Unfortunately, KDI, inc. has recently informed us that they no longer make this model; however, if we can find similar models made by other companies they are preferable. In general, it appears that waveguide phase shifters are less lossy than coax ones. Space considerations aside, it may be beneficial to use waveguide phase shifters with attached coax transitions. For now, we are assuming the phase shifters will have an insertion loss of 1.5 dB each.

5.5 180 Degree Hybrid

The hybrid acts as the "pseudocorrelator" in the receiver. It combines the signals from both chains, averaging out gain fluctuations. The combined signals are then split, and one is shifted in phase relative to the other. We need a 180° hybrid with coax, preferably SMA, inputs and outputs. Anaren offers one for $350 with 0.6dB insertion loss and 43 K noise temperature. Because this component comes after both amplifications, noise temperature is not as important a factor as before.

5.6 Detection

At the detection stage, the antenna power is given by

$$W = Gk_B T_{sys} \Delta\nu, \tag{34}$$

so we need to obtain diodes that yield a square-law response at this power. For an order-of-magnitude estimate, we use the following values:

$G \approx 8.3 \times 10^6$
$k_B = 1.38 \times 10^{-23}$
$T_{sys} \approx 21.23$K
$\Delta\nu = 2 \times 10^8$Hz.

These values give an expected input power of -33.1 dBm, so we probably need diodes that provide a square-law response at -40 dBm or below. We have placed an order at Herotek for a matched pair of diode detectors.

5.7 Component Summary

Figure 2 below shows a summary of what we know so far about the needed components. The estimated system gain is given by

Component	Gain	Insertion Loss	Noise Temp. (K)	Cost	Manufacturer
OMT	.95	≈ 0.2	14	Negligible	GEM students
1^{st} stage amp	1995	0.2dB	3.6	\$3450	Miteq
Phase shifter	≈ 0.7	1.5	120	unknown	Miteq
Filter	.7	≤ 1.5 dB	120	\$895	Trilitihic
2^{nd} stage amp	10000	2 dB	169	\$864	Quinstar
Hybrid/"Magic Tee"	.87	.6dB	43	\$350	Anaren

Table 2: Estimated component parameters.

$$G_{tot} = G_{OMT} \times G_{1^{st}stage} \times G_{2^{nd}stage} \times G_{Filter} \times G_{Phase} \times G_T. \qquad (35)$$

If we assume a .2 dB insertion loss for the OMT, this yields a total gain of 5.85×10^6.

Neglecting the temperature of the horn and assuming the 5.6K/foot temperature

of the SMA cable given in the specifications, the total system temperature is

$$T_{sys} = T_{SMA} + T_{OMT} + \frac{T_{amp1}}{G_{OMT}} + \frac{T_{amp2}}{G_{OMT} \times G_{amp1}} + \frac{T_{filter}}{G_{amp1} \times G_{OMT} \times G_{amp2}} + \frac{T_{Phaseshift}}{G_{filter} \times G_{amp1} \times G_{OMT} \times G_{amp2}} + T_{CMB} + T_{atmosphere} + ...negligible \quad (36)$$

This gives us a T_{sys} of 21.23 K. We do not know the gain or noise temperatures of the OMT and phase shifters, but we can establish upper limits on them. We have previously discussed our needed sensitivity in §3.1. If the largest rms fluctuations we can deal with are

$$\Delta T_{rms} \approx \frac{T_{Amin}}{2} \approx 0.5\text{mK} \quad (37)$$

then we have to achieve a low enough system temperature such that this sky signal can be detected. Using the parameters above, and assuming correlated gain fluctuations average to zero in the hybrid, we have

$$\Delta T_{rms} = 0.98\text{mK}. \quad (38)$$

We are optimistic that this value may be reduced by the following methods:

- Use of a lock-in amplifier. Even a 5dB improvement in signal-to-noise ratio will allow us sufficient temperature sensitivity to detect polarized synchrotron components at the galactic center.

- Separating the first and second stage amplifiers such that gain fluctuations can be treated as uncorrelated. This will produce a minor improvement in temperature sensitivity.

- Attempting to manufacture an OMT with minimal loss, preferably on the order of .1 dB. The graph in Figure 6 shows the estimated dependence of sensitivity on T_{OMT}. We hope to obtain this stability by manufacturing a custom OMT with minimal cross-polarization and low loss.

- Increasing integration time- perhaps by taking data over two or more observing seasons. However, unless gain fluctuations are uncorrelated and can be ignored, increasing the integration time will have little effect.

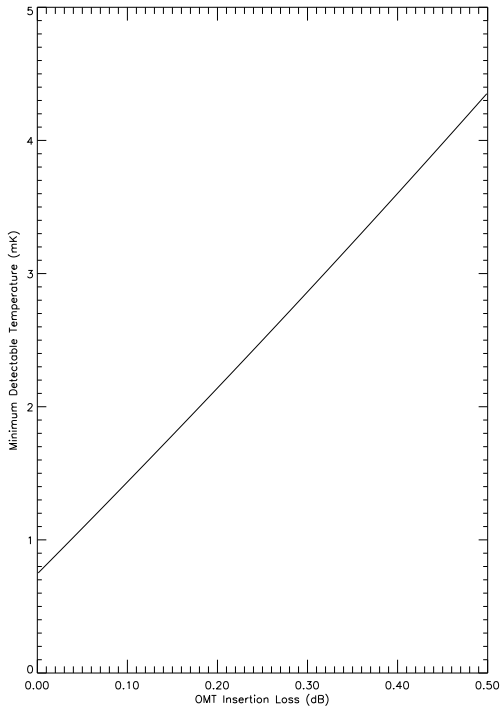

Figure 6: T_{min} versus T_{OMT}.

5.8 Gain Fluctuations

The DAS takes $\approx .4$ seconds to integrate a frame. We do not want the gain to change significantly during this time. So, we need to limit gain fluctuations $\frac{\Delta G}{G}$ to be on the order of $\sqrt{\frac{1}{\Delta\nu\tau}}$ where τ =1 sec. This means that gain fluctuations should be $\leq 7.071 \times 10^{-5}$. The allowable fluctuations per component are displayed in Table 3. Because we will be sampling the signal multiple times per frame, we can get away with larger gain fluctuations, if they are unavoidable. Obviously, though, this will decrease the overall sensitivity.

Component	Allowed ΔG
1^{st} stage amp	$\pm$ .07
Filter	$\pm 2 \times 10^{-5}$
2^{nd} stage amp	$\pm .035$
Phase Shifter	$\pm 1.98 \times 10^{-5}$
Hybrid	$\pm 3 \times 10^{-5}$

Table 3: Allowed gain fluctuations.

6 Computing

6.1 The Data Acquisition System

In order to transmit data digitally, we use standard RS-232 serial port protocol. There are numerous disadvantages to this rather antiquated method, and a redesign of the system is in the works. The Data Acquisition System (DAS) we use consists of a control module, an analog multiplexer/analog-to-digital converter (ADC) module and a serial - to -RS-232 standard output module. This is roughly diagrammed in Fig. 7 below.

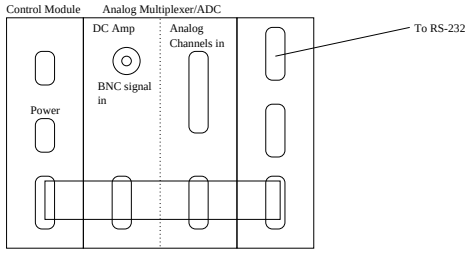

Figure 7: The GEM data acquisition system (DAS)

The control module is connected to the DAS power supply- it requires $\pm$ 15 volts for operation (Gibson, [4]). It is very important to note that the power supply ground will not necessarily be connected to the computer chassis ground, and it is important to make sure that they agree so that the serial port is not blown out. The module has a slide switch to set the baud rate. This is the rate at which data is sent to the

computer, as measured in bits per second. Possible settings range from 150 to 38.4 kbaud.

The most important element in the control module is the EPROM chip, which may be programmed to send data to the serial port in a synchronized manner. To program the EPROM, we use an ancient HT running an antiquated DOS system. An EPROM, or Erasable Programmable Read-Only Memory, chip may be programmed with specific device addresses. This allows our data to be organized and sent serially in a predetermined fashion (Prochnow, [13]). We use a microcomputer to program the chip; this allows us to transmit the data and address locations to the EPROM for writing. We use 267C4 EPROMs with a 64K-bit memory structure; this is more than sufficient for our needs. A typical EPROM program is displayed in Table 4.

EPROM Address	Function	Hex Code
00	Sync Word	00
01	Frame Number MSB	02
02	Frame Number LSB	03
03	Raw Signal	10
04	Integrated Signal	11
05	Low-passed Signal	12
06	Box Temperature	13
07	Integrator Reset	07
08	Integrator Reset	07
09	Dummy Word	FE
10	End of Frame	06

Table 4: Sample EPROM program.

To program an EPROM for the DAS, we first familiarize ourselves with the device address book. This can be found in the DAS documentation. The first element in any program needs to be the "sync word". This is a nonsense word generated by the system that signals the start or end of a frame. Because our data is sent serially,

we must have some intrinsic way to denote the frame. Our sync "word" is EB90 in hexadecimal. Traditionally, the second and third addresses burnt onto the EPROM correspond to the frame number most significant and least significant bit. Following this start, we can then load the addresses of expected signals onto the chip.

On the current DAS, analog channels 1-3 correspond to the input analog signal itself. To simulate a sky signal from the GEM telescope's horn, we often use a low-power signal generator. Channel 1 is the raw signal; this is the received signal from the horn. Channel 2 is the integrated signal. To reduce noise in each frame, we integrate the signal using a simple op-amp circuit inside the DAS module itself. Finally, the signal is passed through a simple low-pass filter to eliminate further effects. The integrated signal data is received on Channel 3.

We utilize the remaining analog channels for "housekeeping" data. These channels may be connected to the temperature control circuitry to keep an accurate record of such important data as ambient temperature, plate temperature, dewar status, etc. Typically, the program is designed to maximize the number of signal samples taken per frame in order to reduce noise. The length of a frame is determined by the baud rate and by observing considerations. We want to make sure that we are sampling the signal at least twice per cycle, and we do not want to degrade frame resolution.

To physically burn the device addresses onto the chip, we use the MOD-MEP-1A/4A/8A high speed EPROM programmer. This program allows us to select the type and operating voltage, and to use a simple text editor to enter in the new program. Burning the new information onto the chip takes about five minutes. To erase an EPROM, it must be exposed to ultraviolet light for a significant amount of time. When erased, all data in the EPROM return to their highest state- FF in HEX. This is a convenient way to check the status of an unknown chip.

The next section of the DAS is the Analog Multi/ADC Module. This device has 16 differential inputs, and is used to convert analog inputs into data suitable for read-in with the PC. If more than 16 inputs are desired, there is an additional Sub-multiplexer module, which has 16 more inputs. The degree of user control possible with these sections of the DAS is significantly less than with the Control Module.

There is an embedded EPROM; this is equipped with a standard program and conforms to the device address book. It should not be re-programmed for routine data acquisition.

We can also connect as many Dual Digital Word Modules as necessary. These accept 2 16-bit words, and are useful in recording digital data like the voltages from the shaft encoder used to determine the pointing. In the past, shaft encoder information has been delivered in an arcane format called Gray Code; more information on this can be found in Horowitz and Hill. In lab testing, we do not utilize the Digital Word Module.

Finally, the Serial to RS232 Module synchronizes the serial data to the "sync" word. This occurs at 9.6 kbaud. Because the conversion of each word to RS232 format takes a certain amount of time, the maximum DAS baud rate is 2.4 kbaud.

6.2 Labview Software

To read in the DAS output, we use an analysis package called Labview. This allows us to easily convert the RS232 standard output into a format usable for analysis. The first element in the Labview program is a function designed to determine how many bytes the main program will read at a time. The function searches incoming data for the "sync word" (235,144 in decimal) and identifies the number of bytes sandwiched between two successive occurrences of the word. The acquisition program is then set to read this many bytes at a time.

Next, the data enters the main portion of the program. This gradually converts the data from RS232 format to an ASCII text file containing the voltage outputs for all 16 analog channels, as well as the frame number. To convert to actual voltages, we note that most interesting data requires at least two bytes, giving us a total of $2^{16} = 65536$ possible voltage states. We need to re-center the data and divide by this number, which should give us voltages to use in analysis.

7 Conclusions

Progress on GEM has been substantially accelerated in the past few weeks, and we expect it to continue throughout the summer and next year. The following are the tasks that have been started and are our current priorities:

1. Construction and testing of the OMT. Working from the design shown, we intend to machine a part and test it by late June.
2. Work on the mechanical housing for the component chain
3. Continued testing and possible maintenance of the liquid nitrogen dewar system.
4. Work on software development for data analysis

Many things have gone wrong with the GEM project, but I am confident that this summer and in subsequent years it will begin to produce good data yet again.

References

[1] Balbi et al. astro-ph/0112391

[2] Banday, Anthony. *Fluctuations in the Cosmic Microwave Background.* Ph. D. thesis.

[3] De Zotti et al. astro-ph/990210302

[4] Gibson, John. Technical documentation. Unpublished.

[5] Heiles, Carl. "Radio Astronomy Fundamentals"

[6] Kamionkowski. astro-ph/9611125

[7] Kraus, John D. *Radio Astronomy*

[8] Kovac et al. astro-ph/0209478

[9] Lance, A.L. *Introduction to Microwave Theory and Measurements.*

[10] Longair, Malcolm. *High Energy Astrophysics*

[11] O'Dell, Chris. Ph. D. thesis

[12] Padmanabhan, R. *Structure Formation in the Universe*

[13] Prochnow, Dave. *Experiments with EPROMS*

[14] Rybicki and Lightman, *Radiative Processes in Astrophysics*

[15] Sazhin. astro-ph/011088

[16] Smoot, George. astro-ph/9902201

[17] Smoot et al. 1992 *Astrophys. J.* 396, L1

[18] White, Martin. astro-ph/9810505

[19] White and Hu, http://background.uchicago.edu/ whu/polar/webversion/polar.html 8

[20] Tegmark et al. astro-ph/9905257

[21] Tello et al. astro-ph/0011412

[22] Torres et al. astro-ph/9605060

[23] Torres et al. astro-ph/9605060

[24] Uher, Jaroslaw. *Waveguide Components for Antenna Feed Systems: Theory and CAD*

[25] Whinnery, Ramo, and Van Duser. *Fields and Waves in Communication Electronics.*

[26] White, Martin. astro-ph/9810505

[27] White and Hu, http://background.uchicago.edu/ whu/polar/webversion/polar.html 8

8 Acknowledgements

First, I would like to thank my advisor, George Smoot. I am very grateful for the opportunity to have worked on GEM and for all his support and guidance. Thanks for giving me the opportunity to learn for myself and make my own (often very serious!) mistakes. Dr. Smoot believed in me even when I doubted my own abilities, and always pushed me to do things I never believed I could do.

Camilo Tello has also been an invaluable resource. I thank him for his vast knowledge and incredible dedication to GEM. Camilo is probably the sole reason GEM still exists today, and all future successes of the project should be credited to him.

Most importantly, I want to thank Kevin Chan, who is a brilliant and hardworking researcher and a good friend. I hope Liz, Erica, Liang, and Colleen learn as much as we did, but I wish them smoother sailing. Thanks to the dearly departed, Anjuli, Yaniv, and Rui for a good summer.

Thanks also to Don Backer and Erik Rosolowsky, who taught me everything I know about IDL and radio calibration, to Domingos Barbosa for explaining why anyone should care about polarization, and to Arman and Jim for knowing infinitely more than I ever will.

Last but not least, I want to thank my family and friends for all their love and support.